J. Electrochem. Sci. Eng. **15(3)** (2025) 2656; http://dx.doi.org/10.5599/jese.2656

Open Access : : ISSN 1847-9286
www.jESE-online.org

Original scientific paper

Influence of irradiation treatment on sensing performances of screen-printed electrodes aimed for doxorubicin monitoring

Perica Paunović, Iva Dimitrievska✉, Marija Katerina Paunović, Marija Mitevska and Anita Grozdanov

Ss. Cyril and Methodius University in Skopje, Faculty of Technology and Metallurgy, Rugjer Bošković 16, 1000 Skopje, North Macedonia

Corresponding author: ✉iva@tmf.ukim.edu.mk

Received: January 24, 2025; Accepted: March 20, 2025; Published: March 28, 2025

Abstract

The subject of study is the development of nanosensors based on carbon nanotubes (CNTs) and polyaniline (PANI) aimed at effective detection and monitoring of doxorubicin - a chemotherapy drug used in the treatment of different types of cancer. The main goal is the design of nanosensors that provide precise and reliable detection and monitoring of doxorubicin, providing an effective approach to monitor drug levels during treatment. The research was carried out on the screen-printed electrodes (SPE) with a working electrode of commercial CNTs and PANI and their modification by irradiation with electron irradiation (50 kGy). The structural changes resulting from the e-beam irradiation were observed by scanning electron microscopy, Raman and FTIR spectroscopy, and thermogravimetric analysis. An electrochemical study employing cyclic voltammetry was done to characterize and test the performance of the nanosensors. Modification with electron irradiation was shown as an effective approach to improve the sensing characteristics of the studied SPE, resulting in a lower limit of detection for the modification. The irradiated SPEs exhibit a limit of detection of 12.674 µmol L^{-1} for the modified multi-walled CNT (MWCNT) electrode and 12.712 µmol L^{-1} for the modified PANI electrode, compared to 12.773 µmol L^{-1} for the MWCNT and 12.712 µmol L^{-1} for the PANI commercial electrodes.

Keywords

Electrochemical nanosensors, carbon nanotubes, polyaniline, e-beam irradiation

Introduction

Doxorubicin (DOX) is a potent medication utilized in the treatment of various malignancies, including breast cancer, leukemia, and lung cancer [1]. Its effectiveness arises from its capacity to disrupt the replication processes of cancer cells, ultimately leading to their destruction. However, the therapeutic efficacy of doxorubicin is significantly influenced by the need to maintain optimal drug concentrations in the body. This balance is crucial to maximize its anticancer effects while minimizing potential adverse effects, such as toxicity to healthy tissues. Therefore, monitoring

doxorubicin concentrations is essential, as it allows healthcare professionals to tailor dosage regimens according to the unique pharmacokinetics of each patient. Continuous daily monitoring of drug concentrations in DOX-treated patients is critical.

In recent years, electrochemical sensors have emerged as a promising alternative for the detection and analysis of pharmaceuticals. These sensors present several advantages over conventional analytical methods, including rapid analysis, accuracy, high sensitivity, and portability [2,3]. In contrast, techniques such as liquid chromatography, mass spectrometry, UV-Vis spectroscopy, and FTIR spectroscopy have notable limitations [4-6], such as lengthy analytical times, the requirement for multiple preparative steps, high equipment costs, significant reagent and solvent consumption, and the need for highly skilled personnel. Presently, screen-printing technology has enabled the production of inexpensive, highly sensitive, and reproducible electrodes for a variety of applications. This advancement has made electrochemical sensing a straightforward, rapid, selective, and cost-effective method. The primary steps in the preparation of screen-printed electrodes (SPEs) involve the screen printing of conductive inks, such as metals, carbon nanostructures, conductive polymers, or nanocomposites - onto smooth substrates made of plastic or ceramics, followed by thermal curing [7].

Various electrode materials have been utilized for DOX sensing, including those based on nano-scaled metals [3,8], carbon nanostructures [9-11], conductive polymers [12-14], and nanocomposites [15,16].

Carbon nanotubes (CNTs) are nanostructures known for their superior mechanical, electrical, and surface properties, making them highly suitable materials for screen-printed electrodes (SPEs). In addition to their functional atomic structure, CNTs can interact with other materials, such as metals, complexing agents, polymers, and functional groups, which enhances the functionality and effectiveness of SPE systems [17]. The detection of doxorubicin (DOX) using CNTs electrodes relies on the interaction between π-π stacking and Van der Waals forces between the side walls of CNTs and the aromatic rings of DOX [18,19]. This interaction facilitates the adsorption of DOX onto the CNTs surface, resulting in a more intense electrochemical redox reaction. This intensity is reflected in well-defined and pronounced oxidation and reduction peaks. Hajian *et al.* [10] developed an electrochemical sensor using platinum (Pt) coated with multi-walled carbon nanotubes (MWCNTs) for the detection of DOX in real blood samples. The DOX was effectively adsorbed onto the electrode surface, exhibiting well-shaped redox peaks. Key electrochemical parameters, including pH, buffer type, accumulation time, MWCNT amount, and scan rate, were optimized. Kalambate *et al.* [20] created a sensor for detecting DOX in real blood samples based on mesoporous palladium-platinum (Pd-Pt) core-shell nanoparticles supported on MWCNTs (Pd-Pt/MWCNT). This sensor demonstrated an excellent voltammetric response to DOX. In addition to its outstanding sensing capabilities, this system exhibited high electrical conductivity, a large real surface area, and an appropriate mesoporous core-shell structure suitable for fast electron transfer. Sharifi *et al.* [16] investigated a glassy carbon electrode modified with MWCNTs decorated with gold nanoparticles for the determination of DOX. This nanocomposite displayed efficient catalytic activity for the reduction of DOX, leading to a significant increase in peak current density and a notable reduction in overpotential. Furthermore, the MWCNTs/gold nanoparticles composite exhibited good selectivity, reproducibility, repeatability, and long-term stability. Taei *et al.* [21] utilized a nanocomposite consisting of MWCNTs and magnetic nanoparticles ($CoFe_2O_4$) to create a sensor for detecting DOX by modifying a carbon paste electrode (MWCNTs/$CoFe_2O_4$/CPE). The exceptional sensing performance of this system is attributed to its superparamagnetic properties, nanometer

dimensions, high stability, large surface area-to-volume ratio, and antifouling characteristics toward DOX and its oxidation products. Peng *et al.* [9] developed a MWCNTs/Poly-L-lysine modified SPE for detecting DOX in real clinical blood samples. The electrochemical oxidation peak current was significantly increased due to the presence of nanocomposites. This sensing system for DOX has the potential to effectively monitor therapeutic drug levels for personalized clinical treatment.

PANI (polyaniline) is a type of conductive polymer known for its adjustable electrical conductivity, exceptional biocompatibility, and environmental stability, making it a low-cost and redox-active material. These properties have garnered significant attention for its application in bio or chemical sensors [22,23]. PANI's electrochemical characteristics, including its conductivity across a wide potential range and ability to facilitate redox processes, position it as an excellent candidate for signal transduction in electrochemical sensors. Shamagsumova *et al.* [12] studied a sensor designed for detecting anthracycline anticancer drugs such as doxorubicin, daunorubicin, and idarubicin. This sensor involved a glassy carbon electrode coated with PANI, which was applied via electropolymerization, using native DNA and oxalic acid as doping agents. Impedance and voltammetric measurements indicated that the surface coating exhibited an extended pH range of electrochemical activity. Additionally, the interaction between the sensor and anthracycline drugs led to a decrease in electron transfer resistance and a reduction in the current of the redox probe (ferricyanide anion). In a separate study, Kulikova *et al.* [13] developed a voltammetric sensor based on a glassy carbon electrode coated with PANI and saturated with methylene blue using captured native DNA. The thickness of the PANI coating was controlled by the number of voltammetric cycles and the pH of the solution. They tested this sensor on artificial samples that simulated the ionic content of human serum, as well as on commercial drug formulations containing doxorubicin (DOX). The sensor achieved a recovery rate of 67 % for DOX determination before centrifugation and 82% after centrifugation, demonstrating its potential for detecting residual DOX in blood serum. Furthermore, the same researchers [14] developed another sensor featuring a glassy carbon electrode modified with native DNA, placed between two electropolymerized layers of PANI. The charge transfer resistance at the interface of the inner layer decreased across a DOX concentration range from 1.0 pmol L^{-1} to 0.1 mmol L^{-1}. The applicability of this developed sensor was confirmed by testing spiked samples of artificial urine, which showed acceptable accuracy of signal measurement following pH correction.

When ionizing radiation passes through solid materials, it interacts with atoms on both atomic and crystal levels, leading to structural changes in the material. This interaction primarily manifests as various defects or disorders [24]. In the case of carbon nanotubes (CNTs), two principal processes can occur: i) defect formation and ii) graphitization [25-27]. Ionizing radiation can break the bonds between carbon atoms and cause atoms to sputter from the surface, resulting in the creation of vacancies that can vary from single to multiple. These vacancies, along with interstitials, can induce significant reconstruction of the carbon network, giving rise to in-plane disorders such as pentagons or heptagons [28]. Furthermore, the energy from ionizing radiation can eliminate specific functional groups, allowing for additional carbon atoms to bond in their place, forming new C-C or C=C bonds [27]. This process, known as graphitization, enhances crystallinity, improves thermal stability, and increases electrical conductivity. In the case of polyaniline (PANI), ionizing radiation can induce several effects: i) intermolecular cross-linking, which enhances thermal and mechanical stability; ii) an increase in crystallinity and a reduction in d-spacing, leading to improved electrical conductivity; and iii) a decrease in crystallite size, which increases the effective surface area [29]. Also, the exposure of polymeric material such as PANI to ionizing treatment leads to the creation of highly reactive intermediates, free radicals, ions, and excited species [30].

The focus of this paper is on the structural changes and sensing performance of the anticancer drug doxorubicin (DOX) when combined with e-beam irradiation-modified multi-walled carbon nanotubes (MWCNTs) and polyaniline (PANI) solid polymer electrolyte. This paper makes a novel contribution by conducting an electrochemical study of pure PANI as a sensor for DOX, as well as introducing a new method for modifying CNTs and PANI SPEs through low-energy ionizing radiation, specifically e-beam irradiation.

Experimental

The sensing characteristics of commercial multi-walled carbon nanotubes (MWCNTs) and polyaniline (PANI) screen-printed electrodes (SPEs) from Dropsens Ltd, Spain, were investigated. These commercial electrodes underwent modification through electron beam (e-beam) irradiation. The SPEs were exposed to a linear accelerator (ELU-6, Eksma, Russia), delivering a beam of 6 MeV electrons. The dose rate was calibrated to 100 Gy/s, as determined by polymer film dosimetry (B3000, B3WINdose Dosimeters), culminating in a total absorbed dose of 50 kGy.

The analyte of focus was the anticancer drug doxorubicin, classified as an anthracycline. Pharmaceutical samples of DOX were procured from local pharmacies. For the electrochemical measurements, the electrolyte consisted of DOX dissolved in double-distilled water (with conductivity ≤ 0.1 μS cm^{-1}), combined with a phosphate-buffered solution (PBS). The final composition of the electrolyte was 0.002 μmol L^{-1} DOX mixed with 0.1 μmol L^{-1} PBS at a pH of 6.8. All chemicals utilized were of analytical grade. To determine the limit of detection (LOD) and quantification (LOQ), a calibration curve constructed from 1.5 to 7.4 μmol L^{-1} was used. LOD and LOQ were calculated based on $S/N = 3$ and $S/N = 10$.

The structural changes of irradiated electrochemical sensors were investigated using a range of techniques, including scanning electron microscopy (SEM), Raman spectroscopy, infrared (FTIR) spectroscopy, and thermogravimetric analysis (TGA). SEM imaging of MWCNTs and PANI in both irradiated and non-irradiated solid polymer electrolytes (SPEs) was performed with a JEOL JSM-IT200 Scanning Electron Microscope, applying acceleration voltage of 20 kV and 30 kV. Non-polarized Raman spectra of MWCNTs-based SPEs were acquired using a micro-Raman multichannel spectrometer (Horiba Jobin Yvon LabRam 300 Infinity), employing the Raman effect excited by a 632.8 nm laser line from a He-Ne laser, without the use of a filter. FTIR spectra for the MWCNTs-based systems were recorded on a Perkin Elmer Spectrum 100 machine, capturing 64 scans in attenuated total reflection (ATR) mode over the range of 400 to 4000 cm^{-1}. The thermal stability of both SPE systems was evaluated using a Perkin Elmer PYRIS diamond thermogravimetric/differential thermal analyzer (TGA/DTA/DTG). The measurements took place in an airflow atmosphere, with the samples heated from 25 to 950 °C at a rate of 40 °C min^{-1}.

The electrochemical characterization of the SPEs was conducted using cyclic voltammetry (CV). CV scans were performed at room temperature utilizing the SPELEC potentiostat/galvanostat from DROPSENS, Spain, and were controlled via the Dropview software package. For the MWCNT systems, the potential range was established from -0.1 to +0.6 V, which was similarly applied to the PANI-based systems. To analyze the Tafel plots and the kinetics of the DOX oxidation process, as well as the double-layer capacitance of the electrodes under investigation, cyclic voltammograms were obtained at varying scan rates of 25, 50, 100, 200, and 300 mV/s. After optimization, a scan rate of 25 mV/s was selected for balancing the stability and sensitivity of the reduction and oxidation peaks.

Results and discussion

Structural changes of the MWCNTs and PANI induced by e-beam irradiation

The passage of e-beam irradiation through the electrode materials, specifically MWCNTs and PANI, leads to structural and surface alterations that influence their electrochemical properties. First, consider the structural changes observed in the MWCNT-based SPE. In Figure 1, SEM images of both irradiated and non-irradiated SPEs are shown. The non-irradiated electrode exhibits a relatively smooth surface and a uniform, defect-free structure (Figure 1a). In contrast, following e-beam irradiation, the electrode surface reveals increased roughness (Figure 1b), which suggests an enlarged surface area that enhances its applicability for electrochemical sensing applications.

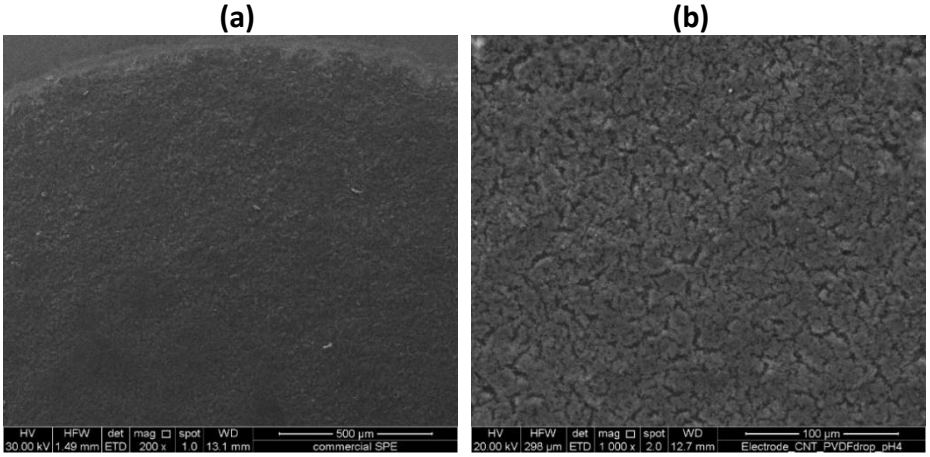

Figure 1. *SEM images of the MWCNTs based SPE systems: (a) before e-beam irradiation and (b) after e-beam irradiation*

In Figure 2, the results of the spectroscopic and thermal analysis are presented. The Raman spectra (Figure 2a) reveal two characteristic peaks associated with MWCNTs: the G peak at approximately 159 cm^{-1} and the D peak at around 1370 cm^{-1}. The G peak corresponds to a high-order as well as a defect-free structure found in Figure 1a, whereas the D peak indicates disorder, which is often attributed to various types of defects and increased surface disorders found in Figure 1b, [31]. The ratio of the intensities of the G and D peaks (I_G/I_D) serves as an indicator of the crystallinity of MWCNTs. Following e-beam irradiation, the I_G/I_D ratio increased from 3.33 to 3.57. This modest increase suggests that defect creation and graphitization occurred, with the latter process somewhat more prominent. These changes have a positive impact on the electrochemical behavior of the electrode. The introduced defects enhance surface roughness, while graphitization improves electrical conductivity. Additional support for the occurrence of graphitization is provided by the FTIR spectra (Figure 2b). The previously low-intensity peak related to C=C bonds at 1610 cm^{-1} shifted to a higher wavelength of 1640 cm^{-1} after irradiation. Furthermore, the symmetric and asymmetric peaks associated with C-H stretching disappeared following irradiation, indicating the formation of additional C-C bonds due to the incorporation of other carbon atoms. Thermo-gravimetric analysis (TGA) illustrated in Figure 2c demonstrated that e-beam irradiation significantly enhanced the thermal stability of MWCNTs by decreasing the oxygen functional groups and increasing their specific surface area as shown also in Figure 1b. As a result of irradiation, an additional graphitization of carbon networks was induced. The irradiated MWCNTs have demonstrated higher thermal stability and the main thermal degradation temperatures were shifted to higher values ($T_{d,MWCNT}$ =681.2 °C; $T_{d,\ MWCNTirrad.}$ = 850.5 °C).

The SEM images of the PANI-based electrodes are illustrated in Figure 3.

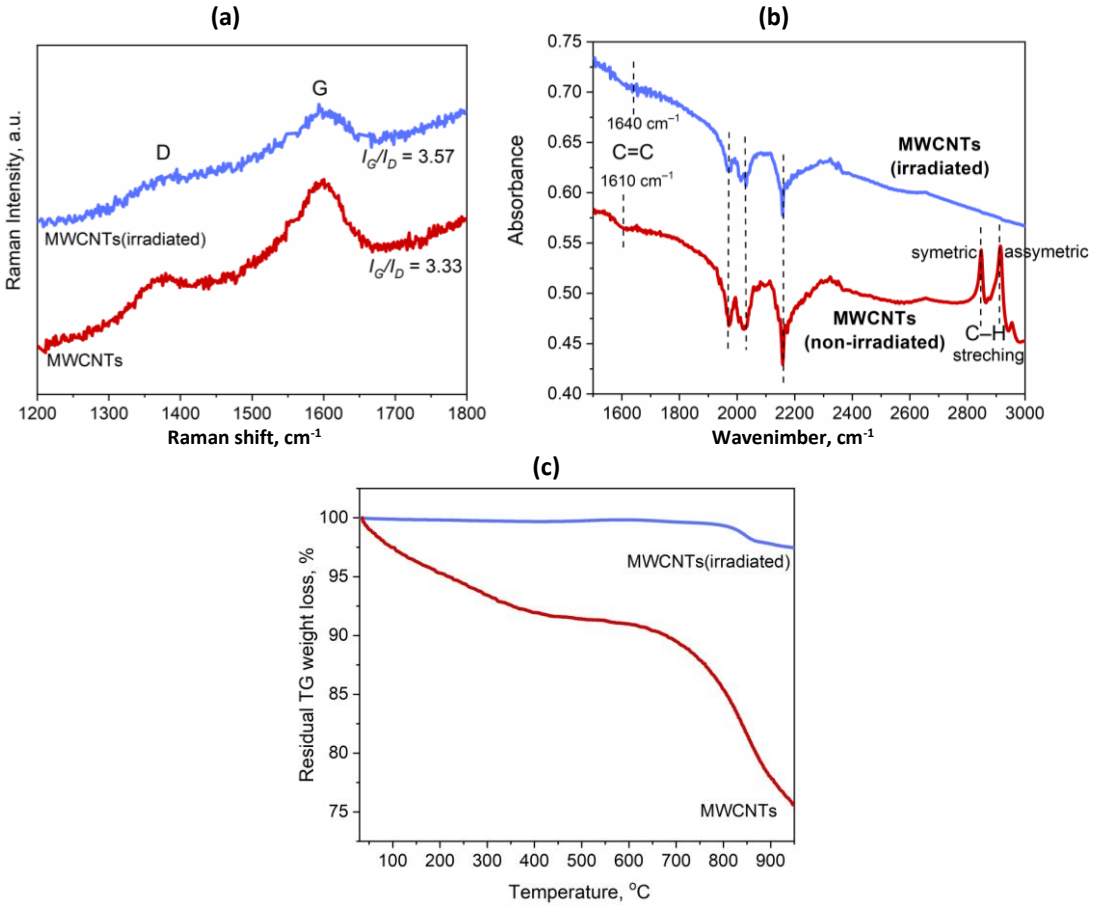

Figure 2. *Structural changes of the MWCNTs-based SPE systems before and after e-beam irradiation analyzed by (a) Raman spectroscopy, (b) FTIR spectroscopy and (c) TG analysis*

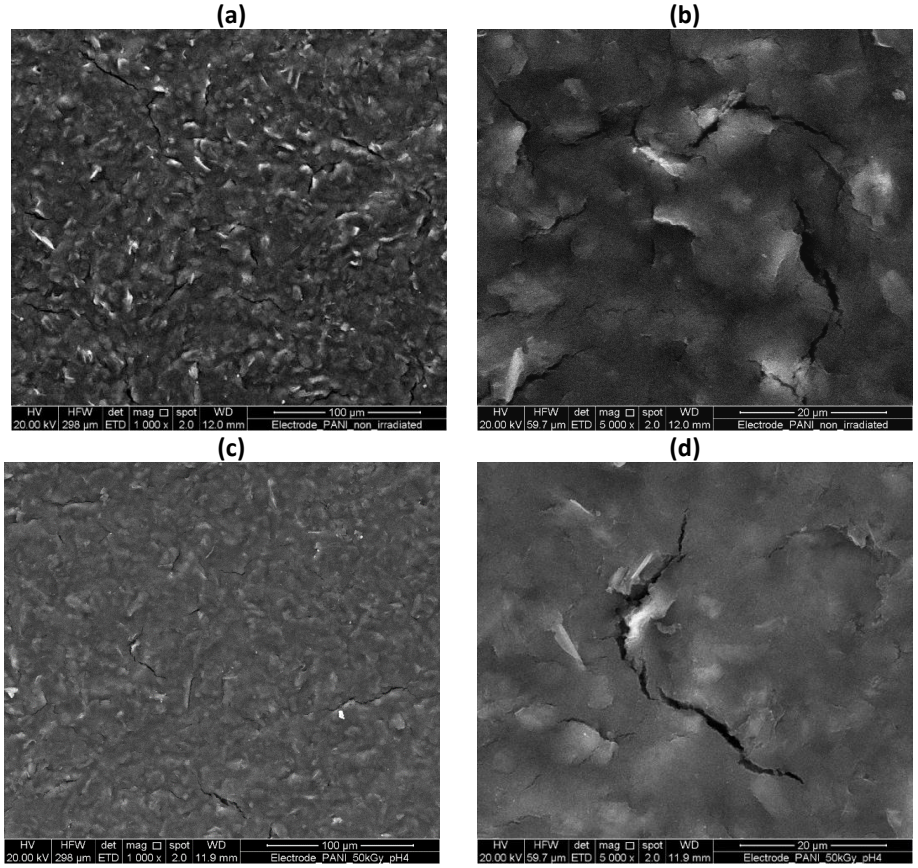

Figure 3. *SEM images of the PANIs-based SPE systems: (a,b) before e-beam irradiation and (c,d) after e-beam irradiation*

The non-irradiated electrodes display agglomerates and micro-cracks resulting from the manufacturing process. In contrast, the microstructure of the irradiated electrodes shows that e-beam irradiation has a detrimental effect on the electrode surface. This process increases the existing microporosity, thereby enhancing the electrode's real surface area.

As demonstrated in Figure 4, the thermal stability of the irradiated electrode has significantly improved. This enhancement can be attributed to the molecular cross-linking during the e-beam irradiation process related to the changes in the TGA curve of irradiated PANI, which exhibited degradation slopes around 350 and 480 °C [29].

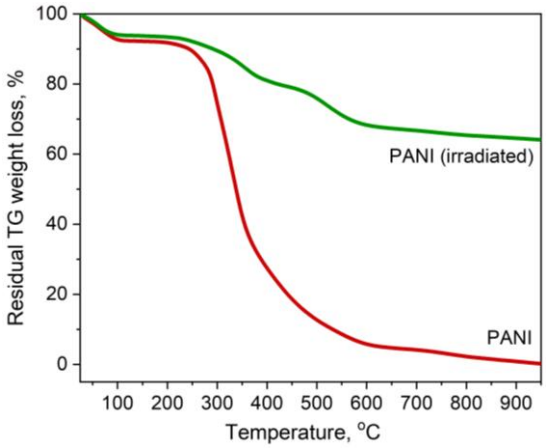

Figure 4. *TGA diagram of the PANIs-based SPE systems before and after e-beam irradiation*

Cyclic voltammetry

The sensitivity of commercial SPEs based on CNTs and PANI, along with modified SPEs treated with an electron beam at a dose of 50 kGy, was assessed for the detection of doxorubicin (DOX). Electrochemical measurements were conducted using cyclic voltammetry in an electrolyte comprising 4 ml of DOX and 20 ml of phosphate-buffered saline (PBS) at pH 6.8. The pH value was specifically chosen to mimic the range of human blood, ensuring that the fluid used for all measurements closely reflects real-life application conditions. The cyclic voltammetry (CV) measurements facilitate the detection of distinct oxidation-reduction (redox) reactions occurring on the surfaces of the investigated SPE systems. In the case of the MWCNTs electrode, the sensing signal for DOX detection is generated through interactions involving π-π stacking and Van der Waals forces between the side walls of the MWCNTs and the aromatic rings of DOX [18,19]. For the PANI electrode, the interaction is between the aromatic rings, containing amine (NH_2) and imine (C=O) functional groups, and the functional groups of DOX, with a particular emphasis on the amine (NH_2) groups [32].

The characteristic cyclic voltammograms of the studied sensor systems are presented in Figure 5. All systems demonstrated a strong electrochemical response, evidenced by two well-defined peaks characteristic of DOX redox reactions. The peak in the anodic part of the voltammogram, labeled $P_{ox.}$, corresponds to the oxidation of DOX, while the peak in the cathodic part, labeled $P_{red.}$, represents the reverse reaction—the reduction of the oxidized form back to DOX. This indicates that a reversible reaction takes place on the electrode, occurring in both directions, as illustrated in Figure 5c [33].

In both systems, incorporating MWCNTs and PANI, the electrodes irradiated with an electron beam at a dose of 50 kGy exhibited an enhanced sensing response.

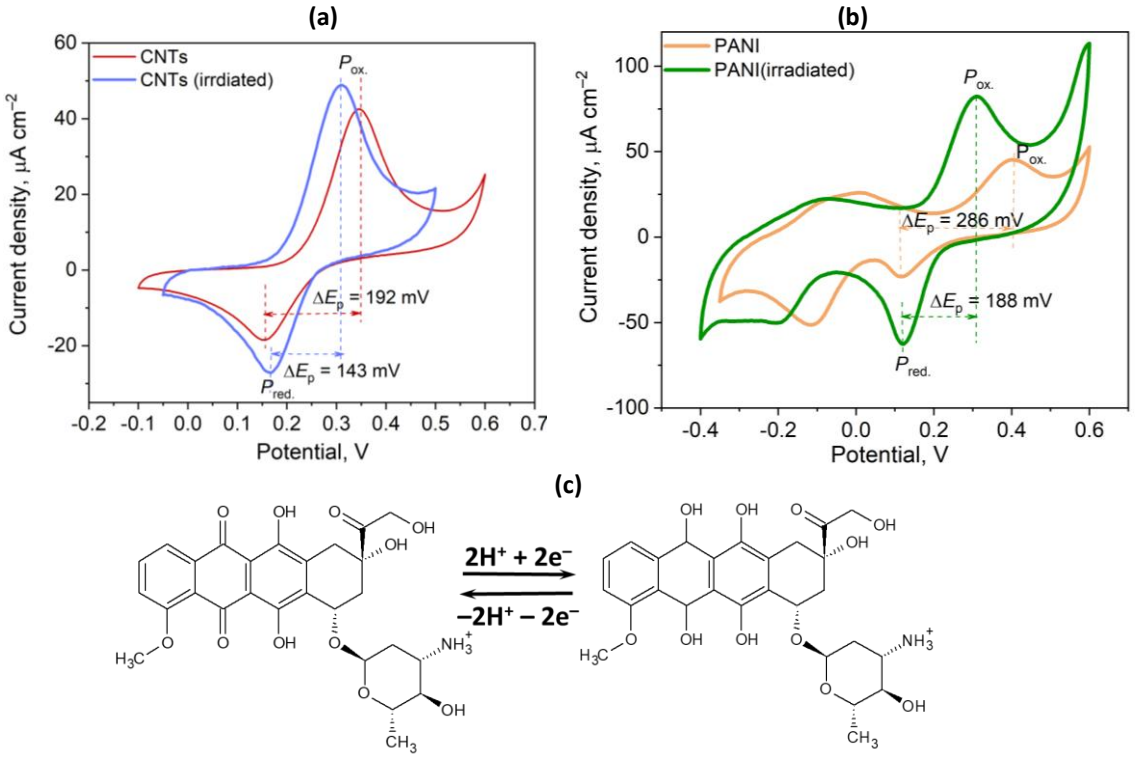

Figure 5. *CVs of the studied electrodes at pH 6.8 and scan rate of 25 mV·s^{-1}: (a) MWCNTs-based systems, (b) PANI-based systems and (c) schematic view of the electrochemical oxidation of DOX*

This improvement is reflected in higher current densities for the corresponding oxidation and reduction peaks ($i_{ox.}$: 49 *vs.* 42 mA cm^{-2} for MWCNTs systems and $i_{ox.}$: 82 *vs.* 45 mA cm^{-2} for PANI systems) compared to the non-irradiated electrodes. Additionally, the potential difference between the anodic (oxidation) and cathodic (reduction) peaks, known as the separation potential (ΔE_p) [34], is significantly lower for irradiated MWCNTs (approximately 50 mV) and PANI (around 100 mV) compared to the non-irradiated systems (Figs. 5a and 5b). This reduction indicates that the reversibility of the redox reaction of DOX increases in both studied systems after irradiation.

The enhanced electrochemical behavior observed in the irradiated MWCNTs and PANI can be attributed to structural and surface changes induced by the electron beam irradiation process. Spectroscopic results (Figure 2) indicate that defect creation and graphitization occur in the case of MWCNTs, with graphitization being the dominant process. This graphitization improves the electrode's conductivity [27], while the defects - such as vacancies, in-plane disorders, and the shortening and thinning of the MWCNTs - help increase the true surface area of the electrode [28,35]. For PANI, the improved electrochemical performance is linked to increased crystallinity and decreased d-spacing resulting from the irradiation, which enhances electrical conductivity [29]. Additionally, there may be increased inter-chain distances [36] and reduced grain sizes [29,36]. Scanning electron microscopy (SEM) analysis confirmed that the electrode surfaces of both systems exhibit increased roughness.

To establish the relationship between the analytical signal, represented by the oxidation peak current ($i_{ox.}$), and the concentration of DOX, cyclic voltammetry measurements were conducted over a concentration range of 1.5 to 10 μmol L^{-1}. Calibration data can be used to calculate sensitivity, limit of detection (LOD), and limit of quantification (LOQ). The linear correlation between $i_{ox.}$ and DOX concentration (C_{DOX}) for both studied SPE systems is illustrated in Figure 6. Notably, the irradiated SPEs in both systems demonstrate greater linearity, resulting in improved sensitivity, LOD, and LOQ. In particular, the PANI-based systems exhibited a more significant enhancement in these

parameters than the MWCNTs-based systems. For instance, the non-irradiated MWCNTs SPE showed a sensitivity of 0.27 µA µmol L^{-1} (R^2 = 0.9799), while this value was slightly changed at 0.25 µA µmol L^{-1} (R^2 = 0.9953) after irradiation. In contrast, for the PANI-based systems, sensitivity was changed from 0.346 (R^2=0.9651) to 0.218 µA µmol L^{-1} (R^2 = 0.9893). The results of irradiated-tested SPE exhibiting the lowest sensitivity were obtained for irradiated PANI-based SPEs, which indicate superior sensitivity among the modified SPE electrodes. Therefore, it seems that the present-tested, irradiated SPE electrode may be a valuable means for making a voltammetric sensor to detect and monitor DOX in clinical laboratories.

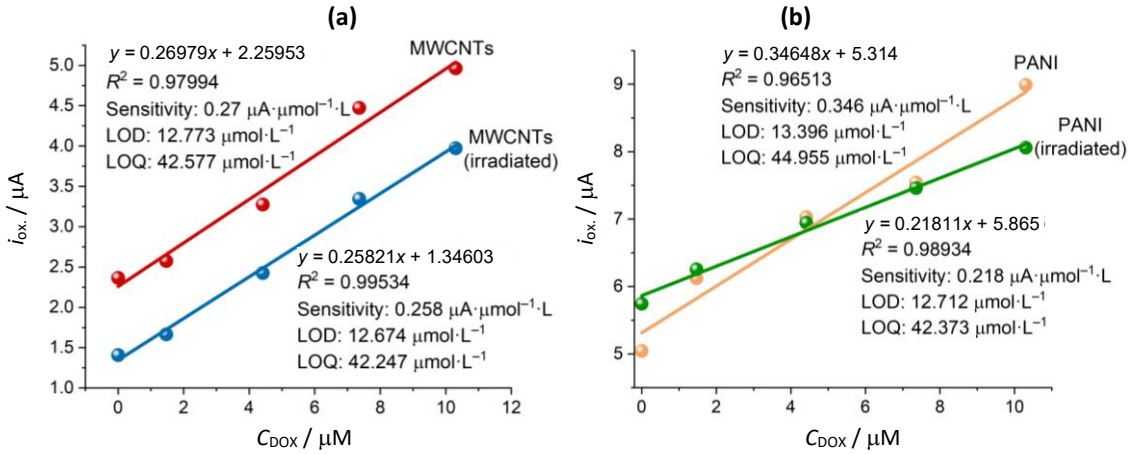

Figure 6. *Linear correlation between the oxidation peak current and DOX concentration for: (a) MWCNTs based system and b) PANI based systems*

Double layer capacity of the electrodes

Cyclic voltammetry scanning conducted at various scan rates v / V s^{-1} enables the determination of double-layer capacitance (C_{dl}), which is directly correlated with the effective surface area of the electrode [37]. A higher C_{dl} value signifies a larger effective surface area of the electrode. The CV voltammograms for all studied electrodes were recorded at different scan rates of 25, 50, 100, 200, and 300 mV s^{-1}, as illustrated in Figure 7. The capacitive current density ($j_{cap.}$) can be calculated as the average of the absolute values of both anodic ($j_{anod.}$) and cathodic ($j_{cat.}$) current densities within the potential range relevant to the charge and discharge of the electrochemical double layer, specifically from the intersections denoted A-A, Equation (1) [38]:

$$j_{cap.} = \frac{|j_{cat.}| + |j_{anod.}|}{2} \quad (1)$$

The relationship between capacitive current density and scanning rate exhibits a linear trend. The slope of this line corresponds to the double-layer capacitance (C_{dl}) of the electrodes under investigation [39,40]. This relationship can be expressed by Equation (2):

$$C_{dl} = \frac{dj_{cap.}}{d(\partial E / \partial t)} = \frac{dj_{cap.}}{dv} \quad (2)$$

where E denotes potential, t represents time, and v is the scanning rate.

The $j_{cap.}$ *vs.* v plots for MWCNTs and PANI SPE systems are presented in Figure 8. It is evident that the irradiated SPEs for both systems exhibited nearly double the values of double-layer capacitance compared to their non-irradiated counterparts (0.096 *vs.* 0.052 mF cm^{-2} for the MWCNTs system and 0.547 *vs.* 0.273 mF cm^{-2} for the PANI system), suggesting a corresponding increase in the effective surface area. This observation further supports the enhanced real surface area induced by

electron beam (e-beam) irradiation, a phenomenon previously corroborated through microscopic and spectroscopic analyses.

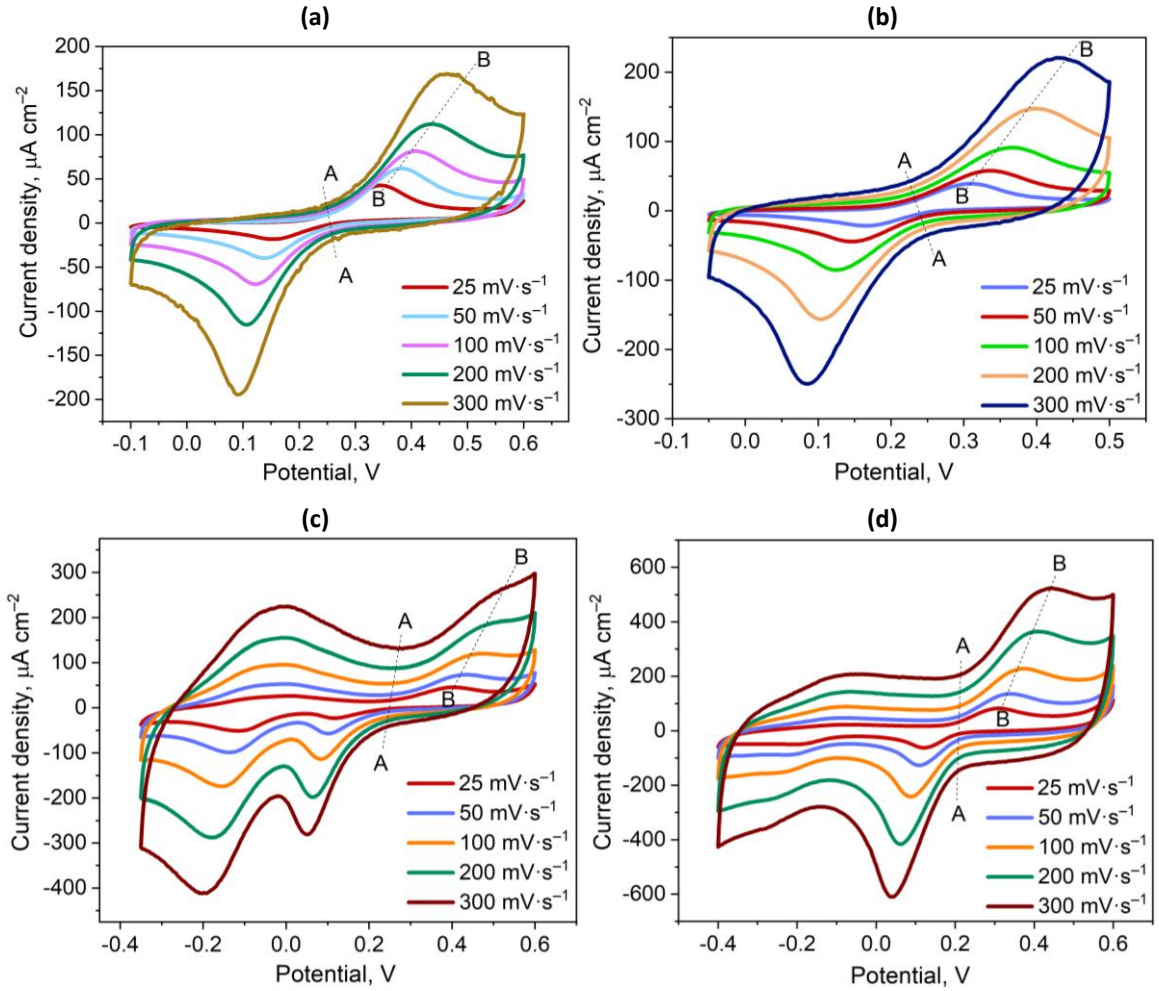

Figure 7. *Cyclic voltammograms obtained at pH 6.8 and different scan rate for: (a) non-irradiated MWCNTs SPE, (b) irradiated MWCNTs SPE, (c) non-irradiated PANI SPE and (d) irradiated PANI SPE*

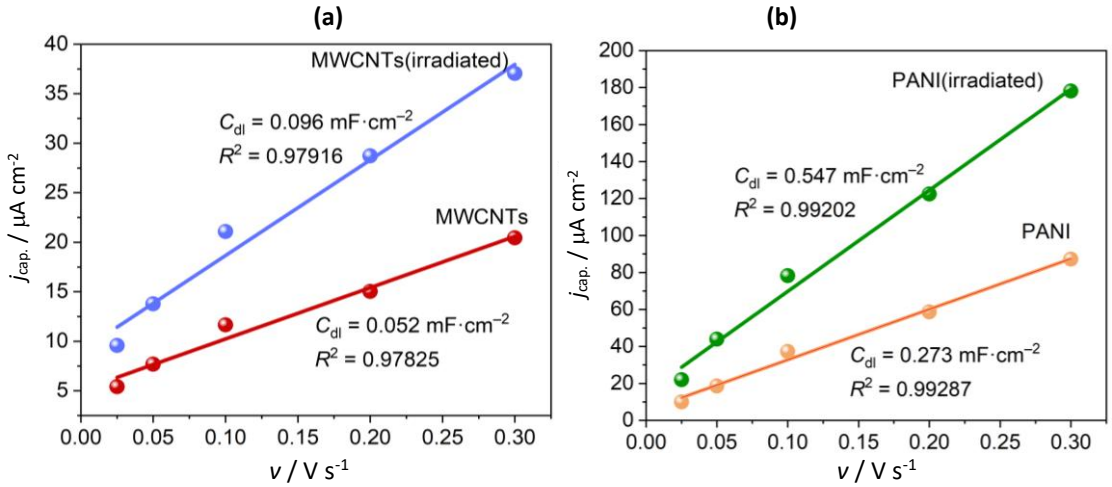

Figure 8. *Linear fit of the plot log* $j_{cap.}$ vs. v *for: (a) MWCNTs based SPEs and (b) PANI-based SPEs*

Specifically, for the MWCNTs, the increased surface area is attributed to the formation of various types of defects (*e.g.* in-plane disorders), as well as the shortening and thinning of the nanotubes. In the case of PANI, the increase in surface area is likely due to the reduction in grain size and the expansion of pre-existing microporosity. These findings were substantiated by the observed

increase in surface roughness in SEM images and the electrochemical measurements of double-layer capacitance.

Mechanism and kinetics of the electrochemical oxidation of DOX

Cyclic voltammograms recorded at varying scan rates, as depicted in Figure 7, can be utilized to ascertain the mechanism parameters of the electrochemical oxidation of DOX, including the Tafel slope (b) and the number of electrons transferred (n_e). These parameters are crucial for identifying the rate-determining step of the electrochemical oxidation process. The Tafel slope can be calculated as a ratio of the peak potential of the electrochemical oxidation of DOX (E_{Pox}) and the logarithm scan rate (v), as is shown in Equation (3) [41,42]:

$$\frac{dE_{Pox}}{d\log v} = \frac{b}{2};\ b = 2 \cdot \frac{dE_{Pox}}{d\log v} \tag{3}$$

The correlation between the E_{Pox} and the logarithm of scan rate (v) exhibits a linear relationship (Figure 9), where the slope corresponds to $dE_{Pox}/d\log v$. The calculated Tafel slope values, derived from the data presented in Figure 9 and Eq. 3, are summarized in Table 1. For the MWCNT systems, the Tafel slope for non-irradiated electrodes is 210 mV dec^{-1}, whereas for irradiated electrodes, it is 216 mV dec^{-1}. In the case of PANI-based systems, the Tafel slope for the non-irradiated electrode is 228 mV dec^{-1}, and for the irradiated one, it is 220 mV dec^{-1}. These Tafel slope values align with existing literature on the electrochemical oxidation of DOX [43], indicating that e-beam irradiation does not alter the mechanism of the electrochemical reaction but rather its rate.

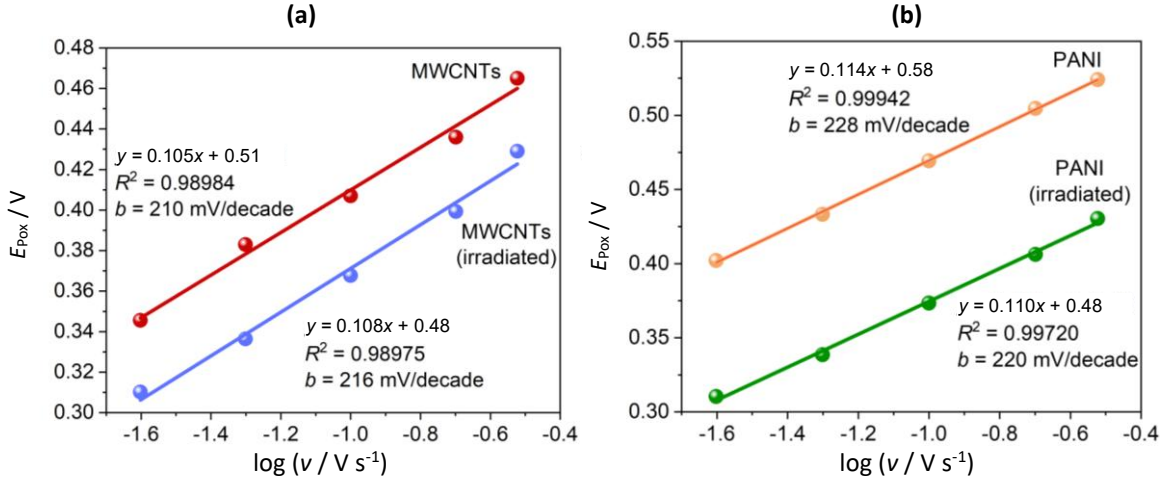

Figure 9. *Linear fit of the plot log* E_{Pox} *vs. log* v *for: (a) MWCNTs-based SPEs and (b) PANI-based SPEs*

Table 1. *Electrochemical parameters calculated for electrochemical oxidation of DOX over the studied SPE systems*

SPE electrode	b / mV dec^{-1}	α	n
MWCNTs	210	0.28	1
MWCNTs (irradiated)	216	0.27	1
PANI	228	0.26	1
PANI (irradiated)	220	0.27	1

The number of electrons involved in the rate-determining step (n_e) can be calculated by the Equation (4) [41]:

$$n_e = \frac{2.303RT}{b\alpha F} \tag{4}$$

where R is the universal gas constant (8.134 J K^{-1} mol^{-1}), T is the temperature (298 K), F is the Faraday constant (96485 C mol^{-1}), and α is the electron transfer coefficient determined by Equation (5) [44]:

$$\alpha = \frac{2.303RT}{bF} \quad (5)$$

The number of transferred electrons (n_e) for all SPEs was determined to be 1. The calculated values of the parameters derived from the aforementioned equations are presented in Table 1. These results suggest that the electrochemical oxidation of DOX in all examined systems is governed by a one-electron transfer process, which is the rate-determining step.

The relationship between the oxidation peak current density (j_{Pox}) and scan rate (v) serves as a criterion for evaluating the kinetics of the process involved in the transfer of reaction species to and from the electrode, which can occur via diffusion or adsorption. A linear correlation between $j_{Pox.}$ and v indicates an adsorption-controlled process, while a linear dependence of $j_{Pox.}$ on $v^{1/2}$ suggests a diffusion-controlled process. However, it is generally observed that the plot of $j_{Pox.}$ *vs.* $v^{1/2}$ tends to exhibit a stronger linear correlation. So, the plot of log $j_{Pox.}$ *vs.* log v is the most reliable and definitive criterion for determining the reaction mechanism [45]. The slope of the log $j_{Pox.}$ *vs.* log v plot serves as an indicator of the predominant reaction mechanism. A slope of 0.5 is characteristic of a diffusion-controlled process, while a slope between 0.5 and 1.0 suggests a process limited by slow adsorption [46,47]. The log $j_{Pox.}$ *vs.* log v plots, derived from the corresponding cyclic voltammograms (Figure 7), are shown in Figure 10. For the MWCNTs-based systems, the slopes were determined to be 0.522 for the non-irradiated SPE and 0.688 for the irradiated SPE. The slope of 0.522, close to 0.5, suggests that the rate-determining step is diffusion-controlled. In contrast, the slope of 0.688 indicates that the process is adsorption-controlled. This kinetic behavior for the non-irradiated electrode can be attributed to the weak adherence of the reaction species to the electrode surface [45]. Previous studies have shown that after electron-beam irradiation, the available surface area for adsorption increases, leading to stronger adherence of the reaction species and a shift in the rate-determining step to one that is adsorption-controlled (as evidenced by the slope of 0.688). For the PANI-based electrodes, the slopes were found to be 0.708 for the non-irradiated SPE and 0.736 for the irradiated SPE, both of which suggest that the rate-determining step (rds) of the process is adsorption.

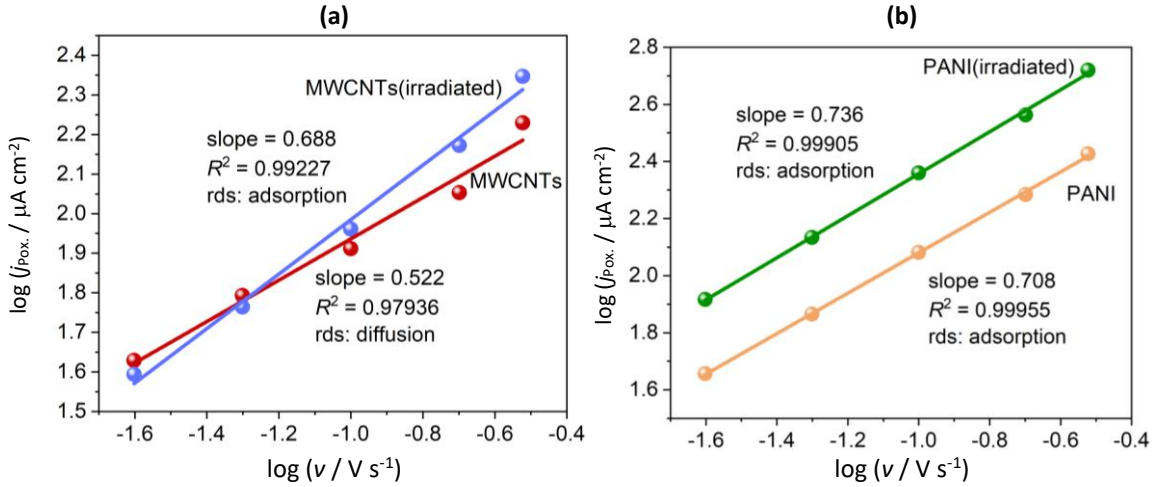

Figure 10. *Linear fit of the plot log* j_{Pox} vs. *log* v *for: (a) MWCNTs based SPEs and (b) PANI based SPEs*

Conclusions

This research was motivated by the idea of developing a fast, simple, and cost-effective method utilizing screen-printed electrodes (SPEs) for the highly sensitive detection of the anticancer drug

doxorubicin (DOX). The commercial MWCNTs and PANI-based SPEs were modified through e-beam irradiation to enhance their sensing performance. Based on the results presented, the following conclusions can be drawn:

- Both systems under investigation (MWCNTs and PANI) demonstrated significant sensitivity for the detection of DOX, as evidenced by well-defined, intense, and prominent oxidation/reduction peaks.
- The e-beam irradiation induced structural and surface changes within the MWCNTs, including defect creation and graphitization.
- The e-beam irradiation also resulted in structural and surface modifications in PANI, such as bond breakage or cross-linking, an increase in crystallinity, a decrease in d-spacing, and a reduction in crystallite size.
- These structural alterations contributed to enhanced thermal and mechanical stability, improved electrical conductivity, a larger real surface area, and, consequently, superior sensing performance for DOX detection.
- The studied SPE systems demonstrated appropriate selectivity, current response, and reproducibility, positioning them as suitable electrodes for sensitive, rapid, and cost-effective detection of DOX.

The innovative combination of the analyte, materials, and modification strategy in this research has not been previously reported.

Acknowledgements*: This paper was realized within the bilateral scientific project between the Faculty of Technology and Metallurgy, Ss. Cyril and Methodius University in Skopje and Montanuniversität Leoben - Department Kunststofftechnik, Austria, supported by the Ministry of Education and Science of the Republic of North Macedonia.*

References

[1] K. I. Popov, S. S. Djokić, N. D. Nikolić, V. D. Jović, *Morphology of Electrochemically and Chemically Deposited Metals*; Springer, New York, USA, 2016, pp. 1-368. https://doi.org/10.1007/978-3-319-26073-0.

[2] Making Metal Powder, https://www.mpif.org/IntrotoPM/MakingMetalPowder.aspx. (accessed on 04 February 2025)

[3] M. Amiri, S. Nouhi, Y. Azizian-Kalandaragh, Facile synthesis of silver nanostructures by using various deposition potential and time: A nonenzymatic sensors for hydrogen peroxide, *Materials Chemistry and Physics* **155** (2015) 129-135. https://doi.org/10.1016/j.matchemphys.2015.02.009

[4] G. Orhan, G. Hapci, Effect of Electrolysis Parameters on the Morphologies of Copper Powder Obtained in a Rotating Cylinder Electrode Cell, *Powder Technology* **201** (2010) 57-63. https://doi.org/10.1016/j.powtec.2010.03.003

[5] N. D. Nikolić, Influence of the exchange current density and overpotential for hydrogen evolution reaction on the shape of electrolytically produced disperse forms, *Journal of Electrochemical Science and Engineering* **10** (2020) 111-126. https://doi.org/10.5599/jese.707

[6] N. D. Nikolić, V. M. Maksimović, Lj. Avramović, Correlation of Morphology and Crystal Structure of Metal Powders Produced by Electrolysis Processes, *Metals* **11** (2021) 859. https://doi.org/10.3390/met11060859

[7] F. C. Walsh, C. T. J. Low, A review of developments in the electrodeposition of tin, *Surface and Coatings Technology* **288** (2016) 79-94. https://doi.org/10.1016/j.surfcoat.2015.12.081

[8] A. W. Lodge, M. M. Hasan, P. N. Bartlett, R. Beanland, A. L. Hector, R. J. Kashtiban, W. Levason, G. Reid, J. Sloan, D. C. Smith, W. Zhang, Electrodeposition of tin nanowires from a

dichloromethane based electrolyte, *RSC Advances* **8** (2018) 24013-24020. https://doi.org/10.1039/C8RA03183E

[9] Z. Wang, J. Ru, Y. Hua, J.Bu, X. Geng, W. Zhang, Electrodeposition of Sn powders with pyramid chain and dendrite structures in deep eutectic solvent: roles of current density and $SnCl_2$ concentration, *Journal of Solid State Electrochemistry* **25** (2021) 1111-1120. https://doi.org/10.1007/s10008-020-04894-7

[10] Z. Wang, J. Ru, Y. Hua, D. Wang, J. Bu, Morphology-Controlled Preparation of Sn Powders by Electrodeposition in Deep Eutectic Solvent as Anodes for Lithium Ion Batteries, *Journal of The Electrochemical Society* **167** (2020) 082504. https://doi.org/10.1149/1945-7111/ab8824

[11] J. Ru, Y. Hua, C. Xu, J. Li, Y. Li, D. Wang, C. Qi, Y. Jie, Morphology-controlled preparation of lead powders by electrodeposition from different PbO-containing choline chloride-urea deep eutectic solvent, *Applied Surface Science* **335** (2015) 153-159. http://dx.doi.org/10.1016/j.apsusc.2015.02.045

[12] J. Ru, J. Bu, Z. Wang, Y. Hua, D. Wang, Eco-friendly and facile electrochemical synthesis of sub-micrometer lead powders in deep eutectic solvents using galena as a raw material, *Journal of Applied Electrochemistry* **49** (2019) 369-377. https://doi.org/10.1007/s10800-018-01284-w

[13] V. S. Cvetković, N. M. Vukićević, N. D. Nikolić, G. Branković, T. S. Barudžija, J. N. Jovićević, Formation of needle-like and honeycomb-like magnesium oxide/hydroxide structures by electrodeposition from magnesium nitrate melts, *Electrochimica Acta* **268** (2018) 494-502. https://doi.org/10.1016/j.electacta.2018.02.121

[14] V. S. Cvetković, N. M. Vukićević, N. D. Nikolić, Z. Baščarević, T. S. Barudžija, J. N. Jovićević, A possible mechanism of formation of flower-like $MgO/Mg(OH)_2$ structures by galvanostatic molten salt electrolysis: The concept of local diffusion fields, *Journal of Electroanalytical Chemistry* **842** (2019) 168-175. https://doi.org/10.1016/j.jelechem.2019.04.067

[15] V. M. Lipkin, L. N. Fesenko, S. M. Lipkin, Tin Powders Electrodeposition from Choline Chloride Based Ionic Liquid, *Solid State Phenomena* **284** (2018) 1252-1256. https://doi.org/10.4028/www.scientific.net/ssp.284.1252

[16] Y. Ni, Y. Zhang, J. Hong, Hierarchical Pb microstructures: a facile electrochemical synthesis, shape evolution and influencing factors, *CrystEngComm* **13** (2011) 934-940. https://doi.org/10.1039/C0CE00272K

[17] R. Sivasubramanian, M. V. Sangaranarayanan, Electrodeposition of silver nanostructures: from polygons to dendrites, *CrystEngComm* **15** (2013) 2052-2056. https://doi.org/10.1039/C3CE26886A

[18] Lj. Avramović, E. R. Ivanović, V. M. Maksimović, M. M. Pavlović, M. Vuković, J. S. Stevanović, N. D. Nikolić, Correlation between Crystal Structure and Morphology of Potentiostatically Electrodeposited Silver Dendritic Nanostructures, *Transactions of Nonferrous Metals Society of China* **28** (2018) 1903-1912. https://doi.org/10.1016/S1003-6326(18)64835-6

[19] M. Yang, W. Xia, J. An, N. Wu, W. Yang, H. Wang, Fractal growth of copper powder on point and plate electrodes based on diffusion-limited aggregation model, *Ionics* **30** (2024) 4313-4323. https://doi.org/10.1007/s11581-024-05554-w

[20] N. Wu, C. Zhang, S. Han, J. An, W. Xia, Effect of Electrolysis Parameters on the Fractal Structure of Electrodeposited Copper, *Journal of Electrochemical Science and Technology* **14** (2023) 194-204. https://doi.org/10.33961/jecst.2022.00878

[21] H.-C. Shin, J. Dong, M. Liu, Nanoporous Structures Prepared by an Electrochemical Deposition Process, *Advanced Materials* **15** (2003) 1610-1614. https://doi.org/10.1002/adma.200305160

[22] T.-H. Kim, K.-S. Hong, D. R. Sohn, M. J. Kim, D.-H. Nam, E. A. Cho, H. S. Kwon, One-step synthesis of multilayered 2D Sn nanodendrites as a high-performance anode material for Na-ion

batteries, *Journal of Materials Chemistry A* **5** (2017) 20304-20315. https://doi.org/10.1039/C7TA06469A
[23] N. D. Nikolić, J. D. Lović, V. M. Maksimović, P .M. Živković, Morphology and structure of electrolytically synthesized tin dendritic nanostructures, *Metals* **12** (2022) 1201. https://doi.org/10.3390/met12071201
[24] N. D. Nikolić, P. M. Živković, J. D. Lović, G. Branković, Application of the general theory of disperse deposits formation in an investigation of mechanism of zinc electrodeposition from the alkaline electrolytes, *Journal of Electroanalytical Chemistry* **785** (2017) 65-74. https://doi.org/10.1016/j.jelechem.2016.12.024
[25] S. J. Banik, R. Akolkar, Suppressing Dendritic Growth during Alkaline Zinc Electrodeposition using Polyethylenimine Additive, *Electrochimica Acta* **179** (2015) 475-481. https://doi.org/10.1016/j.electacta.2014.12.100
[26] J. Rosen, G. S. Hutchings, Q. Lu, R. V. Forest, A. Moore, F. Jiao, Electrodeposited Zn Dendrites with Enhanced CO Selectivity for Electrocatalytic CO_2 Reduction, *ACS Catalysis* **5** (2015) 4586−4591. https://doi.org/10.1021/acscatal.5b00922
[27] P. Lertsathitphong, S. Limpijumnong, M. Somasundrum, A. P. O'Mullane, B. Lertanantawong, Electrochemical Formation of Pb Microwires with Tunable Morphology on Liquid Metal Electrodes, *ACS Omega* **9** (2024) 45641-45650. https://doi.org/10.1021/acsomega.4c09165
[28] V. D. Jović, B. M. Jović, M. G. Pavlović, Electrodeposition of Ni, Co and Ni-Co alloy powders, *Electrochimica Acta* **51** (2006) 5468-5477. https://doi.org/10.1016/j.electacta.2006.02.022
[29] N. D. Nikolić, Lj. Avramović, E. R. Ivanović, V. M. Maksimović, Z. Baščarević, N. Ignjatović, Comparative morphological and crystallographic analysis of copper powders obtained under different electrolysis conditions, *Transactions of Nonferrous Metals Society of China* **29** (2019) 1275-1284. https://doi.org/10.1016/s1003-6326(19)65034-x
[30] D. Desai, X. Wei, D. A. Steingart, S. Banerjee, Electrodeposition of preferentially oriented zinc for flow-assisted alkaline batteries, *Journal of Power Sources* **256** (2014) 145-152. https://doi.org/10.1016/j.jpowsour.2014.01.026
[31] N. D. Nikolić, V. M. Maksimović, G. Branković, P. M. Živković, M. G. Pavlović, Correlation between crystal orientation and morphology of electrolytically produced powder particles: analysis of the limiting cases, *Materials Protection* **59** (2018) 256-264. https://doi.org/10.5937/ZasMat1802256N
[32] D. Perdana, S. Wahyudi, M. Z. Mubarok, Analysis of the Particle Size and Morphology of Tin Powder Synthesized by the Electrolytic Method, *ACS Omega* **9** (2024) 3276-3286. https://doi.org/10.1021/acsomega.3c05179
[33] W. Lou,W. Cai, P. Li, J. Su, S. Zheng, Y. Zhang, W. Jin, Additives-assisted electrodeposition of fine spherical copper powder from sulfuric acid solution, *Powder Technology* **326** (2018) 84-88. https://doi.org/10.1016/j.powtec.2017.12.060
[34] N. D. Nikolić, G. Branković, M. G. Pavlović, Formation of the honeycomb-like electrodes by the regime of pulsating overpotential in the second range, *Journal of Electrochemical Science and Engineering* **2** (2012) 33-40. https://doi.org/10.5599/jese.2012.0009
[35] N. D. Nikolić, G. Branković, M. G. Pavlović, Correlate Between Morphology of Powder Particles Obtained by the Different Regimes of Electrolysis and the Quantity of Evolved Hydrogen, *Powder Technology* **221** (2012) 271-277. https://doi.org/10.1016/j.powtec.2012.01.014
[36] R. K. Nekouei, F. Rashchi, N. N. Joda, Effect of organic additives on synthesis of copper nano powders by pulsing electrolysis, *Powder Technology* **237** (2013) 554-561. https://doi.org/10.1016/j.powtec.2012.12.046
[37] R. Winand, Electrodeposition of metals and alloys - new results and perspectives, *Electrochimica Acta* **39** (1994) 1091-1105. https://doi.org/10.1016/0013-4686(94)E0023-S

[38] C. S. Barrett, T. B. Massalski, *Structure of Metals, Crystallographic Methods, Principles and Data, International Series on Materials Science and Technology*, Pergamon, New York, USA, 1980. ISBN: 008026171X, 9780080261713, pp. 1-654.
[39] X. Zheng, T. Ahmad, W. Chen, Challenges and strategies on Zn electrodeposition for stable Zn-ion batteries, *Energy Storage Materials* **39** (2021) 365-394. https://doi.org/10.1016/j.ensm.2021.04.027
[40] M. N. Kozicki, Information in electrodeposited dendrites, *Advances in Physics: X* **6** (2021) 1920846. https://doi.org/10.1080/23746149.2021.1920846
[41] G. Wranglen, Dendrites and Growth Layers in the Electrocrystallization of Metals, *Electrochimica Acta* **2** (1960) 130-146. https://doi.org/10.1016/0013-4686(60)87010-7
[42] M. V. Mandke, S-H. Han, H. M. Pathan, Growth of silver dendritic nanostructures via electrochemical route, *CrystEngComm* **14** (2012) 86-89. https://doi.org/10.1039/C1CE05791J
[43] J. M. Zhang, F. Ma, K. W. Xu, Calculation of the surface energy of FCC metals with modified embedded-atom method, *Applied Surface Science* **229** (2004) 34-42. https://doi.org/10.1016/j.apsusc.2003.09.050
[44] S. G. Wang, E. K. Tian, C. W. Lung, Surface Energy of Arbitrary Crystal Plane of bcc and fcc Metals, *Journal of Physics and Chemistry of Solids* **61** (2000) 1295-1300. https://doi.org/10.1016/S0022-3697(99)00415-1
[45] H. Fu, L. Xiong, W. Han, M. Wang, Y. J. Kim, X. Li, W. Yang, G. Liu, Highly active crystal planes-oriented texture for reversible high-performance Zn metal batteries, *Energy Storage Materials* **51** (2022) 550-558. https://doi.org/10.1016/j.ensm.2022.06.057
[46] X. Wang, J. P. Meng, X. G. Lin, Y. D. Yang, S. Zhou, Y. P. Wang, A. Q. Pan, Stable zinc metal anodes with textured crystal faces and functional zinc compound coatings, *Advanced Functional Materials* **31** (2021) 2106114. https://doi.org/10.1002/adfm.202106114.
[47] J. O.'M. Bockris, A. K. N. Reddy, M. E. Gamboa-Aldeco, *Modern Electrochemistry 2A, Fundamentals of Electrodics*, Springer, New York, USA, 2000, p. 1333 https://doi.org/10.1007/b113922
[48] N. D. Nikolić, J. D. Lović, V. M. Maksimović, N. S. Vuković, N. L. Ignjatović, P. M. Živković, S. I. Stevanović, Correlation Between Morphology and Crystal Structure of Electrolytically Produced Zinc Dendritic Particles, *Metals* **14** (2024) 1468. https://doi.org/10.3390/met14121468